

# Three-Dimensional Particle-in-Cell Modeling of Parametric Instabilities Near the Quarter-Critical Density in Plasmas

H. Wen,<sup>1,2</sup> A. V. Maximov,<sup>1,2</sup> R. Yan,<sup>1,2,\*</sup> J. Li,<sup>1,2,†</sup> C. Ren,<sup>1,2,3</sup> and F. S. Tsung<sup>4</sup>

<sup>1</sup>Laboratory for Laser Energetics, University of Rochester

<sup>2</sup>Department of Mechanical Engineering, University of Rochester

<sup>3</sup>Department of Physics and Astronomy, University of Rochester

<sup>4</sup>Department of Physics and Astronomy, University of California, Los Angeles

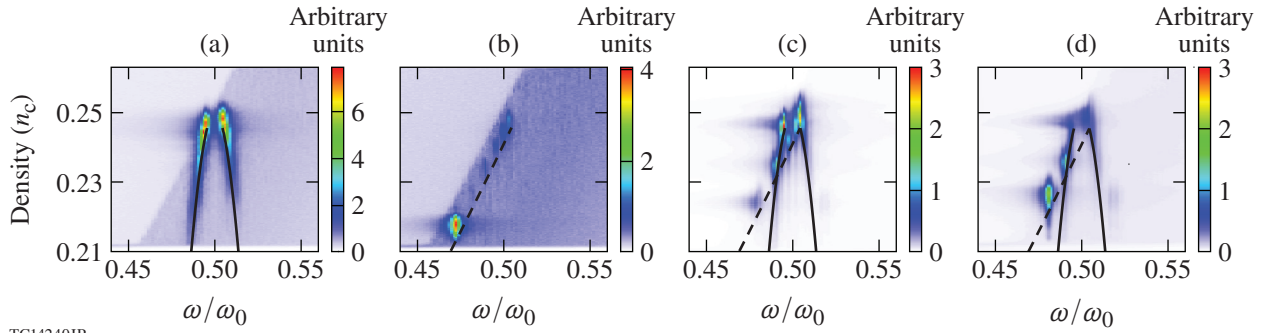
\*Present Address: University of Science and Technology of China

†Present Address: University of California, San Diego

The interplay between two-plasmon decay (TPD) and stimulated Raman scattering (SRS) is studied using particle-in-cell (PIC) modeling in three dimensions. The TPD-related waves are mostly localized in the plane of polarization,<sup>1</sup> which is defined by the incident laser wave vector (in the  $x$  direction) and the laser electric-field vector (in the  $y$  direction). The SRS sidescattering develops mostly outside of the polarization plane, and its scattered-light wave vector is almost perpendicular to the incident laser wave vector.<sup>2,3</sup> Scattered-light waves can also propagate in the direction parallel or antiparallel to the laser wave vector (forward- and backscattering, respectively).<sup>4</sup> A 2-D simulation in the polarization plane ( $x$ - $y$ ) or in the perpendicular plane ( $x$ - $z$ ) will be referred to as  $p$  polarized (PP) or  $s$  polarized (SP), respectively. Two-dimensional simulations can model only the interaction where either TPD (in PP) or SRS (in SP) dominates, except for the high-frequency hybrid instability<sup>5</sup> case when the SRS-scattered light propagates in the backward direction and the SRS-related and TPD-related waves are in the same ( $x$ - $y$ ) plane. The 3-D simulations are required to study the interaction including both TPD and SRS. Here the results of several 3-D simulations for different plasma parameters and incident laser profiles are presented and compared with the respective 2-D simulations to illustrate that both TPD and SRS strongly influence the laser-plasma interaction near-quarter-critical density ( $1/4 n_c$ ). In the 3-D modeling including both TPD and SRS, the fast-electron flux is reduced by up to an order of magnitude compared to 2-D TPD simulation results published earlier.<sup>6</sup>

Here we describe in detail a 3-D simulation for the parameters relevant to inertial confinement fusion (ICF) experiments.<sup>7,8</sup> A CH plasma is initialized with the electron temperature  $T_e = 2$  keV and the temperatures for both ion species,  $T_i = 1$  keV. The incident laser beam with intensity  $I = 9 \times 10^{14}$  W/cm<sup>2</sup> propagates in the direction of density inhomogeneity ( $x$ ). A linear density profile with the scale length  $L = 100 \mu\text{m}$  is assumed at the initial time. The size of the simulation box is  $21 \mu\text{m} \times 8.4 \mu\text{m} \times 6.7 \mu\text{m}$  modeling the density range from  $0.21 n_c$  to  $0.26 n_c$ . Two 2-D simulations (PP and SP) with the same physical parameters were also performed. The TPD threshold parameter  $\eta$  (Ref. 1) is 1.9 ( $\eta = 1$  at threshold), and the SRS backscattering threshold parameter  $N$  (Ref. 4) is 0.5 ( $N = 0.26$  at threshold) for these simulations. The SRS sidescattering threshold<sup>2,3</sup> is close to the backscattering threshold. Both absolute TPD and absolute SRS instabilities are expected to grow. The threshold of the convective SRS<sup>2</sup> is not exceeded for the parameters described above.

The spectra of plasma waves ( $|E_L|$ ) obtained at a time interval between 0.3 ps and 1.0 ps in the 2-D PP and SP simulations are plotted in Figs. 1(a) and 1(b), respectively. From the 3-D simulation, the spectra of plasma waves at a time interval between 1.3 ps and 2.0 ps are plotted in Fig. 1(c) (close to the  $k_z = 0$  plane, where TPD dominates) and in Fig. 1(d) (far away from the  $k_z = 0$  plane, where SRS dominates). One can see from Figs. 1(c) and 1(d) that TPD and SRS coexist near  $1/4 n_c$ . The spectra of the unstable modes for TPD and SRS are close to the linear theory results (see overlaid lines in Fig. 1).



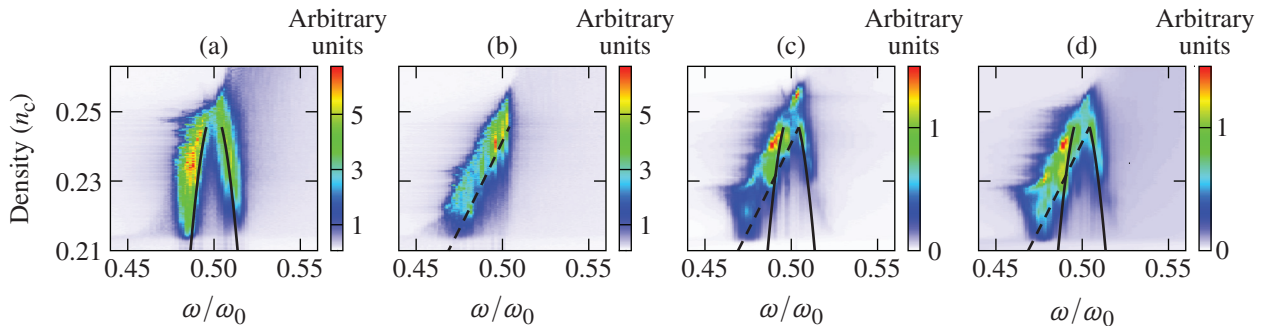
TC14240JR

Figure 1

(a) Plasma-wave spectra in the linear instability stage as a function of plasma density and the wave frequency normalized to laser frequency in 2-D PP, (b) 2-D SP, and (c) 3-D simulation for modes with  $0 \leq k_z/k_0 < 0.2$  and (d)  $0.2 \leq k_z/k_0 < 3$ . The overlaid solid black lines and the dashed black lines represent the dispersion relations satisfying the matching conditions for TPD and SRS, respectively.

As the instability evolves from the linear stage to the saturation stage, the frequency spectra shown in Fig. 1 evolve into the spectra shown in Fig. 2. One can see that the spectra in all these simulations are broader in the saturation stage compared to the linear stage. The density in Fig. 2 is calculated using the initial density profile. Compared to 2-D PP [Fig. 2(a)], the TPD is much weaker at densities lower than  $0.23 n_c$  in the 3-D simulation [Fig. 2(c)]. The weakening of the TPD modes at these densities is also illustrated in Fig. 3(a) [and Fig. 3(b)], where the spectrum of plasma waves at densities below  $0.23 n_c$  in the saturation stage is integrated over  $k_z$  (and  $k_y$ ). There are no prominent modes along the TPD hyperbola<sup>9</sup> [solid black line in Fig. 3(a)] at  $k_x > k_0$ , which corresponds to the TPD daughter waves with larger wave vectors. Two types of low-frequency density fluctuations are identified in our simulations [see Fig. 3(c)]: one type is the ion-acoustic wave, driven by the Langmuir-decay instability (LDI),<sup>10,11</sup> and the other type is driven with the beating of the same-frequency daughter waves of SRS and TPD. The LDI modes form a broad feature at  $k_x \approx 1.7 k_0$  (about  $2 \times$  the laser wave vector in plasma) in the spectrum of the ion density fluctuations shown in Fig. 3(c). The beating of the SRS plasmons with wave vector  $(k_x, k_y, k_z) = (0.87 k_0, 0, \pm 0.2 k_0)$  creates density perturbations  $\langle \delta n \rangle$  with wave vector  $(k_x, k_z) = (0, \pm 0.4 k_0)$ . The coupling between SRS plasmons and  $\langle \delta n \rangle$  generates higher-order modes in the field at  $k_z = \pm(0.2 + m0.4 k_0)$ , [ $m = 1, 2 \dots$ , see Fig. 3(b)] and in the density perturbation at  $(k_x, k_z) = [0, \pm(0.4 + m0.4 k_0)]$  [see Fig. 3(c)].

Although SRS and TPD grow independently in the linear stage, in the nonlinear stage they interact through low-frequency density perturbations. TPD growth starts from the region near  $1/4 n_c$  and spreads to lower densities.<sup>6</sup> Although the peak values of  $\langle \delta n \rangle$  are similar in 2-D and 3-D simulations, the peaks are reached at different densities in different simulations: in 2-D PP (without SRS)  $\langle \delta n \rangle$  peaks at densities where absolute TPD modes dominate (around  $0.245 n_c$ ); in 3-D (with both SRS and TPD)



TC14241JR

Figure 2

Plasma-wave spectra in the saturation stage in the 2-D (from 3.3 ps to 4.1 ps) and 3-D (from 2.3 ps to 3.1 ps) simulations as a function of plasma density and wave frequency. Each panel displays the same quantity as in Fig. 1.

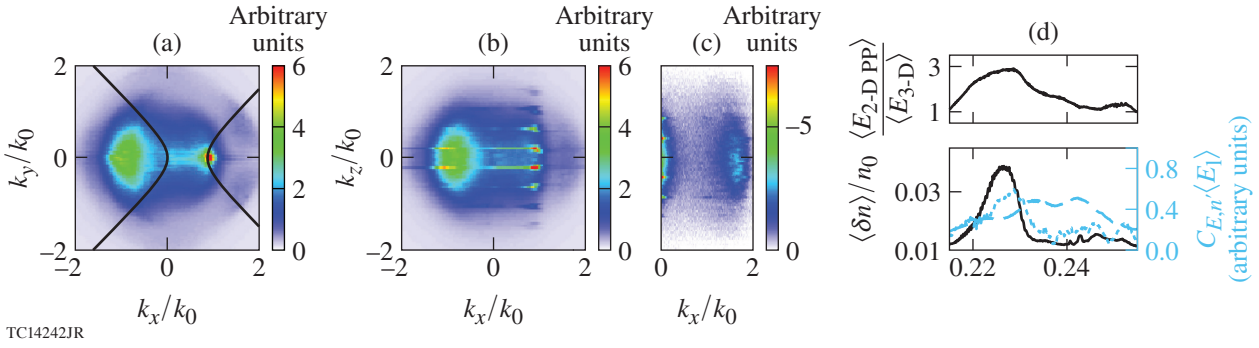


Figure 3

(a) The spectrum of plasmons in the saturation stage of 3-D simulation at densities lower than  $0.23 n_c$  plotted in the  $k_x$ - $k_y$  plane and (b) the  $k_x$ - $k_z$  plane. (c) The spectrum of ion density fluctuation plotted in the  $k_x$ - $k_z$  plane on a logarithmic scale. (d) Lower panel: Ion density fluctuations rms (root-mean-square average over the transverse direction and time) normalized to background density (solid black line), longitudinal electric field rms (dashed blue line) and caviton correlator  $C_{E,n}$  (dotted blue line). Upper panel: the ratio of the electric-field amplitude of the TPD plasmons with larger wave vector between 2-D PP and 3-D simulations.

$\langle \delta n \rangle$  peaks at densities where the frequencies of TPD and SRS plasmons are close. In this region where the dispersion lines for TPD and SRS plasmons intersect [near  $0.23 n_c$  in our simulations; see Figs. 2(c) and 3(d)] multiple pairs of SRS and TPD daughter waves have close frequencies and can drive  $\langle \delta n \rangle$  through the ponderomotive force to much higher levels compared to other density regions [see the black line in Fig. 3(d)]. The level of  $\langle \delta n \rangle$  near  $0.23 n_c$  is lower in 2-D PP than in 3-D simulations. In the 3-D simulation the growth of TPD plasmons at densities below  $0.23 n_c$ , seeded by plasmons from above  $0.23 n_c$ , is disrupted by these enhanced ion density perturbations, as illustrated by a decrease in the level of TPD-driven plasmons below  $0.23 n_c$  in Fig. 2(c).

The correlation between the local plasmon intensity  $|E_L|^2$  and the density fluctuations  $\delta n$  is captured using the caviton correlator<sup>12</sup>

$$C_{E,n} = \langle -\delta n |E_L|^2 \rangle / \left[ \langle (\delta n)^2 \rangle \langle E_L^2 \rangle / 2 \right].$$

As shown in the lower panel of Fig. 3(d), the plasma waves and the density fluctuations are weakly correlated between  $0.255 n_c$  and  $0.235 n_c$ :  $C_{E,n} = 0.1$  to  $0.2$  in spite of a significant level of plasmons in this density range. At densities close to  $0.23 n_c$ , the lower panel of Fig. 3(d) shows the increase not only in the plasmon intensity and density fluctuations, but also in the correlation between them with  $C_{E,n}$  reaching up to  $0.6$ . The large caviton correlator indicates that the plasma waves are strongest in areas where density is depleted. The ponderomotive force of multiple pairs of SRS and TPD daughter waves with close frequencies is responsible for driving the enhanced density perturbations. The nonlinear coupling of TPD and SRS through ion perturbations leads to a lower TPD saturation level in the 3-D simulation compared to the 2-D PP simulation, which is illustrated in the upper panel of Fig. 3(d).

The fast-electron flux is defined as the energy flux carried by electrons with kinetic energy above  $55$  keV leaving the simulation box minus the energy flux carried by the thermal electrons injected into the simulation region from the thermal boundaries (in the  $x$  direction). Information about the hot electrons is collected during the saturation stage in each simulation for  $0.5$  ps. In the 3-D simulation, the fast-electron flux associated with the forward- and backward-going hot electrons was found to be  $1.7\%$  and  $0.8\%$ , respectively. The plasma-wave spectrum in the 3-D simulation corresponds to a smaller  $k$ -space domain than the spectrum in 2-D PP, which makes the staged acceleration mechanism less efficient in 3-D than in 2-D and explains a smaller number of hot electrons in the 3-D simulation compared to 2-D PP ( $6.6\%$  and  $3.4\%$  in the forward and backward directions, respectively). The influence of wave breaking on the fast-electron generation is small because the maximal electric field amplitude ( $0.04 m_e \omega_0 c/e$ ) is below the wave-breaking limit ( $0.1 m_e \omega_0 c/e$ ) (Ref. 13).

The nonlinear regime including both TPD and SRS is also observed in simulations with the speckled laser beam<sup>14,15</sup> and electron-ion collision effects included. In PIC simulations with periodic boundary conditions, the limited-size simulation region

effectively represents a much larger volume of plasmas and the single speckle in the simulation region mirrors itself in the transverse directions. A series of simulations has been performed to study how the speckles affect the generation of hot electrons. All parameters are the same as the simulations described previously except for the temperatures of electrons and ions being  $1.5\times$  higher. The peak intensities in the laser speckles are  $1.8 \times 10^{15} \text{ W/cm}^2$  (twice the average intensities). A collision package (CP) is available for the PIC code *OSIRIS*.<sup>16</sup> The main physics processes are observed to be the same in simulations with plane-wave beams and speckled beams.

The fast-electron flux values in simulations are listed in Table I for different incident laser beams as well as with CP turned on and off. By comparing the left and right columns of Table I, one can see that adding collisions can reduce the fast-electron flux by about 50% and in the case of plane-wave 2-D PP simulation by almost 70%. Also note that the reduction of the fast-electron flux caused by collisions affects both the forward-going electrons and backward-going electrons since the collisional damping rate affects all the plasma waves. The fast-electron flux generated in 2-D SP is much smaller than the fast-electron flux generated in 2-D PP, which indicates that the plasma waves driven by TPD are the main source of the electron acceleration.

Table I: Fast-electron flux normalized to the incident laser energy flux.

Fast-electron flux	Forward/Backward	
	On	Off
Plane wave 2-D PP	1.6% / 1.3%	5.5% / 3.8%
Plane wave 2-D SP	(< 0.1%) / 0.2%	(< 0.1%) / 0.5%
Speckle 2-D PP	6.8% / 1.7%	9.4% / 3.8%
Speckle 2-D SP	(< 0.1%) / 0.3%	(< 0.1%) / 0.7%
Speckle 3-D	0.4% / 0.3%	0.8% / 0.5%

The hot-electron fraction observed in the ICF experiments on the OMEGA Laser System does not exceed a few percent.<sup>8</sup> At the same time, in the previous PIC simulations of TPD in 2-D, the hot-electron fraction was close to an order of magnitude larger than in the experiments. The 3-D PIC simulations presented here produce the results for the hot-electron fraction that are close to the experimental levels.

Laser-plasma interaction near  $1/4 n_c$  determines the generation of fast electrons that are crucial for the performance of ICF targets. The fast-electron flux in simulations is found to be closely related to the plasma-wave spectra. The TPD-driven plasma waves with large wave vectors are very important for accelerating electrons. At the same time, the SRS-driven plasma waves are less effective in accelerating electrons. Therefore the modeling that includes the nonlinear coupling of TPD and SRS in 3-D is the only way to correctly describe the generation of fast electrons in laser-driven ICF.

Our 3-D PIC simulations have shown the large decrease (up to an order of magnitude) in the fast-electron flux compared to 2-D TPD modeling. The reason is the nonlinear coupling between SRS and TPD, which is especially pronounced at densities lower and around  $0.23 n_c$ . In this region, plasma waves and growing density perturbations are localized in the same areas as illustrated by the caviton correlator. Enhanced density perturbations detune and weaken the TPD-driven plasmons effective in the fast-electron generation. In addition to the TPD suppression, the plasma-wave spectra in 3-D simulations are much more narrow compared to the spectra in 2-D TPD modeling. To conclude, 3-D PIC simulations presented in this summary fully model the laser-plasma interaction near  $1/4 n_c$ , including SRS and TPD, and obtain the fast-electron fraction level close to experimental results, resolving the large discrepancy between ICF experiments and PIC simulations that have existed for many years.

This work was supported by the Department of Energy National Nuclear Security Administration under Award Number DE-NA0003856, the University of Rochester, and the New York State Energy Research and Development Authority. We also acknowledge the support by the DOE under grant No. DE-SC0012316, and by the NSF under grant No. PHY-1314734.

1. A. Simon *et al.*, Phys. Fluids **26**, 3107 (1983).
2. C. S. Liu, M. N. Rosenbluth, and R. B. White, Phys. Fluids **17**, 1211 (1974).
3. B. B. Afeyan and E. A. Williams, Phys. Plasmas **4**, 3803 (1997).
4. J. F. Drake and Y. C. Lee, Phys. Rev. Lett. **31**, 1197 (1973).
5. B. B. Afeyan and E. A. Williams, Phys. Plasmas **4**, 3845 (1997).
6. R. Yan *et al.*, Phys. Rev. Lett. **108**, 175002 (2012).
7. W. Seka *et al.*, Phys. Plasmas **16**, 052701 (2009).
8. D. T. Michel *et al.*, Phys. Plasmas **20**, 055703 (2013).
9. J. Meyer and Y. Zhu, Phys. Rev. Lett. **71**, 2915 (1993).
10. D. F. DuBois and M. V. Goldman, Phys. Rev. **164**, 207 (1967).
11. D. F. DuBois, H. A. Rose, and D. A. Russell, Phys. Scr. **T63**, 16 (1996).
12. H. X. Vu *et al.*, Phys. Plasmas **19**, 102708 (2012).
13. T. P. Coffey, Phys. Fluids **14**, 1402 (1971).
14. Y. Kato *et al.*, Phys. Rev. Lett. **53**, 1057 (1984).
15. S. Skupsky *et al.*, J. Appl. Phys. **66**, 3456 (1989).
16. R. A. Fonseca *et al.*, in *Computational Science – ICCS 2002*, edited by P. M. A. Sloot *et al.*, Lecture Notes in Computer Science, Vol. 2331 (Springer, Berlin, 2002), pp. 342–351.